Acta Oceanol. Sin., 2022, Vol. 41, No. 4, P. 138–145
https://doi.org/10.1007/s13131-021-1842-y
http://www.aosocean.com
E-mail: ocean2@hyxb.org.cn

A novel synthetic aperture radar scattering model for sea surface with breaking waves

Xiaochen Wang[1, 2], Yuxin Hu[1, 2*], Bing Han[1, 2], Wei Tian[1], Chunhua Zhang[3]

[1] Aerospace Information Research Institute, Chinese Academy of Sciences, Beijing 100094, China

[2] Key Laboratory of Technology in Geo-spatial Information Processing and Application System, Chinese Academy of Sciences, Beijing 100190, China

[3] The box 51111, Beijing 100190, China

Received 14 November 2020; accepted 14 April 2021

Abstract

In this study a novel synthetic aperture radar (SAR) scattering model for sea surface with breaking waves is proposed. Compared with existing models, the proposed model considers an empirical relationship between wind speed and wave breaking scattering to present the contribution of wave breaking. Moreover, the scattering weight factor p, and wave breaking rate q, are performed to present the contribution of the quasi-specular scattering term, Bragg scattering term, and wave breaking scattering term to the total scattering from the sea surface. To explore the modeling accuracy of sea-surface scattering, a simulated normalized radar cross-section (NRCS) and measured NRCS are compared. The proposed model generated the simulated NRCS and a matching GF-3 dataset was used for the measured NRCS. It was revealed that the performance of the VV polarization of our model was much better than that of HH polarization, with a correlation of 0.91, bias of –0.14 dB, root mean square error (RMSE) of 1.26 dB, and scattering index (SI) of –0.11. In addition, the novel model is explored and compared with the geophysical model of CMODs and satellite-measured NRCS from GF-3 SAR wave mode imagery. For an incidence angle 40°–41°, the relationship between the NRCS and wind speed, relative wind direction is proposed. As with the SAR-measured NRCS, the performance of VV polarization was much better than HH polarization, with a correlation of 0.99, bias of –0.25 dB, RMSE of 0.64 dB, and SI of –0.04.

Key words: synthetic aperture radar, scattering model, sea surface, wave breaking

Citation: Wang Xiaochen, Hu Yuxin, Han Bing, Tian Wei, Zhang Chunhua. 2022. A novel synthetic aperture radar scattering model for sea surface with breaking waves. Acta Oceanologica Sinica, 41(4): 138–145, doi: 10.1007/s13131-021-1842-y

1 Introduction

Modeling of electromagnetic scattering from the sea surface is significant for active remote sensing of marine dynamics and target detection. Using satellite-launched spaceborne synthetic aperture radar (SAR), it is feasible to retrieve upper sea-surface dynamics of wind, waves, and currents based on the relationship between the SAR normalized radar cross-section (NRCS) of the sea surface and sea states that induce and modulate the sea-surface roughness (Elfouhaily et al., 1997; Hauser et al., 2008; Mouche et al., 2007; Romeiser et al., 1997). Although the orbiting spaceborne SAR can process images of sea state characteristics in response to radar echoes, the contribution of wave breaking on total SAR backscattering from the sea surface is still unclear (Apel, 1994; Hwang et al., 2010). Considering the unsatisfying consistency between SAR-measured and theoretical values, it is still important to explore wave-breaking scattering and develop a novel sea-surface electromagnetic scattering model to better explain the scattering mechanism between observed sea-surface roughness and derived NRCS from SAR imagery.

Since the middle of the 20th century, with the development of spaceborne radar observation technology, the electromagnetic scattering problem of the sea surface has become a compelling research topic. Based on the Maxwell equation, researchers have developed a variety of numerical scattering models using different numerical approximation methods, including Kirchhoff approximation, perturbation method, and small slope approximation. To explore the radar scattering characteristics of the sea surface, the physical optics (PO) model, geometric optics (GO), Bragg scattering model, two-scale model (TSM), three-scale model (MSM), small slope approximation (SSA) and integral expansion method (IEM) are proposed to analyze the NRCS characteristics for difference radar incidence angles (Barrick, 1965; Barrick and Bahar, 1981; Donelan and Pierson, 1987; Plant, 2002; Voronovich, 1994; Wu and Fung, 1972). Theoretically, the different radar responses of the sea surface can be attributed to the backscattering mechanism at different incidence angles. The quasi-specular scattering mechanism dominates in the sea-surface total scattering, whereas at medium incidence angles, the Bragg resonance scattering of free-propagating short waves modulated by long waves dominates in the sea-surface total scattering. However, any single scattering mechanism cannot explain the NRCS characteristics of the sea surface for SAR observation of a continuous incidence angle. To date, there is no clear and unified transition method to combine different scattering models. It also should be noted that the effects of breaking waves on co-pol and cross-pol radar scattering from the sea surface are not considered in the aforementioned model simulations (Hwang and Plant, 2010; Plant and Irisov, 2017).

Foundation item: The National Natural Science Foundation of China under contract No. 4197060692.
*Corresponding author, E-mail: huyx@aircas.ac.cn

Generally, the effect of wave breaking on sea-surface total scattering is neglected for engaged models. At present, the linear wave theory considers that the sea surface can be described as a linear superposition of waves of different scales and ignores the nonlinear part of waves, which brings uncertainty to the study of electromagnetic scattering characteristics of sea surface (Elfouhaily et al., 1997). The nonlinear part of waves is mainly caused by the wave breaking. The wave breaking will form foam and a white crown on the wave crest, especially in high wind-speed sea conditions. The breaking waves will change the radar backscattering of the sea surface, resulting in constrained Bragg scattering, foam scattering, splitting scattering, specular scattering, and multiple scattering (Chubb et al., 1999; Churyumov and Kravtsov, 2000; Helluy et al., 2005). In a previous study, it is reported that the contribution of wave breaking to the sea-surface total scattering component can reach approximately 60%–70% for C-band HH and VH polarizations for all incidence angles. To investigate the physical mechanism of wave-breaking in sea-surface total scattering, some experiential models were proposed to directly establish the relationship between scattering components induced by wave breaking, radar parameters (e.g., incidence angle, polarization), and wind vector (e.g., wind speed, relative wind direction). Compared with C-band quad-polarization RADARSAT-2 SAR data, it has been found that simulations of quad-polarization radar backscatter are significantly improved when the effects of breaking waves are incorporated, especially for HH and VH polarizations (Voronovich and Zavorotny, 2001; Zhang et al., 2020). At present, few studies focus on the co-modeling method with consideration of wave breaking for a continuous incidence angle. To better understand the imaging mechanism of SAR for sea surface, it is important to explore a clear and unified mathematical relations to model each contribution of the physical mechanisms of the sea surface to the sea-surface total scattering (Hauser and Caudal, 1995, 1996).

The contents of this study are organized as follows. In Section 2, the dataset used in this study is briefly introduced, together with the methodology. The experiment is described in Section 3, with a general overview of wave-breaking scattering. Then a novel scattering model with a breaking term is proposed and validated by using GF-3 SAR measurement. Some discussions about model applicability for different bands are given in Section 4. Finally, the conclusions of this study and some future strategies to develop modeling precision are described in Section 5.

2 Data set and methodology

2.1 *Data set*

The GF-3 wave mode imagery was collected from January to March of 2018, in the North Pacific. A total of 2 900 scenes of SAR imagery were taken as measured-NRCS and collocated with a wind vector of U_{10} at a 10 m height above the sea surface, which were provided by European Centre for Medium-Range Weather Forecasts (ECMWF) re-analysis data. The coverage of GF-3 wave mode imagery can provide a 5 km × 5 km swath width for every 50 km along the orbit direction with quad-polarization measurement. The map of the collected GF-3 SAR wave mode imagery is shown in Fig. 1. To collocate the wind field provided by ECMWF, the time and space matching window for collocation was constrained to be smaller than 30 min and 10 km, respectively. The GF-3 SAR measured NRCS was acquired on use of GF-3 radiometric calibration, which follows as:

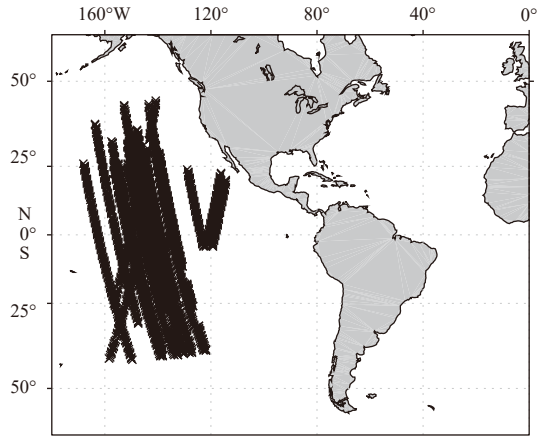

Fig. 1. Map of collected GF-3 SAR wave mode imagery.

$$\sigma^0 = 10\log_{10}\left[(I^2+Q^2)\times\left(\frac{\text{Qualify Value}}{32\,767}\right)^2\right] - K_{\text{dB}}, \quad (1)$$

where σ^0 represent the NRCS in unit of dB, Qualify Value represent the imagery quantization value, K_{dB} represent the calibration const. In addition, considering the inaccuracy of GF-3 SAR calibrated NRCS (Wang et al., 2019; Zhang et al., 2019), the collected data was recalibrated to acquire a precise NRCS by using GF-3 SAR imagery of the same beam position over a rainforest (Li et al., 2019b; Zhong et al., 2020). Moreover, a homogeneity check was performed to exclude the influence of other features (e.g., sea ice, ships, oil spill, biogenic slick) on the sea-surface NRCS caused by wind vectors (Gao et al., 2018).

2.2 *Methodology*

Along with the development of microwave scattering theory, the sea-surface backscattering model is proposed in a number of studies (Plant, 2002; Yan et al., 2018). According to the scattering mechanisms presented in the literature, the ensemble of sea-surface scattering can be the sum of Bragg scattering and non-Bragg scattering.

2.2.1 *Bragg scattering*

At a medium incidence angle, the radar scattering theory of sea surface is based on the Bragg resonance scattering mechanism of random rough sea surface. The sea-surface resonance wavelength and the sea-surface NRCS is highly related with radar wavelength for a constant incidence angle. The resonance wavelength of sea surface verifies the following relationship (Hwang and Plant, 2010):

$$L = \frac{n\cdot\lambda}{2\sin\theta}, \quad (2)$$

where θ and λ are the incidence angle and transmitted radar wavelength; and n represents the n-order Bragg scattering component, which is usually taken as 1. For the pure Bragg scattering, the NRCS is proportional to the Bragg spectral density spectrum, which can be expressed as (Kudryavtsev et al., 2003)

$$\sigma^p_{0br} = 16\pi K^4\left|G_p(\theta)\right|^2 F_r(k_{br},\varphi), \quad (3)$$

where p denotes HH or VV polarization state; G_p is the Bragg scattering coefficient; $k_{br}=2K\sin\theta$ is the Bragg wave number; K

is the radar wave number; θ is the incident angle; and $F_r(k,\varphi)$ is the sea-surface folded symmetry two-dimensional wave number spectrum. The polarization scattering coefficients of VV and HH are expressed as (Plant, 1986)

$$|G_v(\theta)|^2 = \frac{\left(1+\sin^2\theta\right)^2\cos^4\theta}{\left[\cos\theta+0.111\right]^4}, \tag{4}$$

$$|G_h(\theta)|^2 = \frac{\cos^4\theta}{\left[0.111\cos\theta+1\right]^4}. \tag{5}$$

For a given incident angle, the Bragg scattering signal depends on the short-wave spectral density and its azimuth distribution. In real sea conditions, the short-wave Bragg scattering occurs on long waves, and the pure Bragg scattering theory loses its effectiveness. Thus, a composite Bragg scattering model is needed. The model considers that the scattering of each tilted facet on the long wave is Bragg scattering, and the average scattering cross-section is the average of the scattering cross-section of a single small panel on the long wave. When the slope of the long wave is small, the NRCS can be expressed as follows:

$$\sigma_{br}^p = 16\pi K^4 \overline{\left|G_p\left(\theta-\zeta_x,\zeta_y\right)\right|^2 F_r\left(k'_{br},0\right)}. \tag{6}$$

According to a previous study (Kudryavtsev et al., 2003), Eq. (5) can be expanded by following the slope of the long wave, and the function form of second-order expansion is as follows:

$$\sigma_{br}^p(\theta,\varphi) = \sigma_{0br}^p(\theta,\varphi)\left(1+g^p\overline{\zeta_x^2}-\frac{M_{t0}^p}{B_{r0}}\overline{\zeta_x B_r}\right), \tag{7}$$

where σ_{0br}^p is the pure Bragg scattering cross section; $\overline{\zeta_x^2}$ is the x-direction long wave mean square slope (i.e., radar-filtered mean square slope); $M_{t0}^p = \left(1/\sigma_{0br}^p\right)\partial\sigma_{0br}^p/\partial\theta$ is the tilt modulation transfer function; B_r is the short wave spectrum change caused by the interaction between long wave and short wave; and g^p is the polarization coefficient.

$$g^v = \frac{1}{2\sigma_{0br}^v}\frac{\partial^2\sigma_{0br}^v}{\partial\theta^2}, \tag{8}$$

$$g^h = \frac{1}{2\sigma_{0br}^h}\frac{\partial^2\sigma_{0br}^h}{\partial\theta^2} + \frac{2}{\sin^2\theta}\frac{|G_v(\theta)|}{|G_h(\theta)|}\frac{\overline{\zeta_y^2}}{\overline{\zeta_x^2}}. \tag{9}$$

The second term in brackets in Eq. (6) describes the contribution of pure tilt effect, and the third term is the cross-correlation term between tilt effect and hydrodynamic effect, which is the only responsibility term in Eq. (6) to distinguish the backscattering cross-section between upwind and downwind. Figure 2 shows the NRCS of the composite Bragg (CB) scattering model in HH/VV polarization and upwind/crosswind direction compared with radar incidence angle and wind speed.

2.2.2 *Non-Bragg scattering*

At small radar incidence angles, especially at the nadir point of radar measurement footprint, the quasi-specular scattering of sea surface is the main mechanism of generating the sea-surface radar backscattering signal.

$$\sigma_{sp} = |R_{\text{eff}}|^2\pi\sec^4\theta\, p\left(\zeta_{x'},\zeta_{y'}\right), \tag{10}$$

where $p\left(\zeta_{x'},\zeta_{y'}\right)$ is the probability density function of the slope of specular point; $\zeta_{x'} = \tan\theta\cos\phi_w$ and $\zeta_{y'} = -\tan\theta\sin\phi_w$ are the slopes of upwind and crosswind, respectively; and ϕ_w is the angle of wind direction relative to radar beam. By neglecting the difference of the cross-section between upwind and downwind, the slope probability density function can be simplified as Gaussian type:

$$p\left(\zeta_{x'},\zeta_{y'}\right) = \frac{1}{2\pi\overline{\zeta_u\zeta_c}}\exp\left[-\frac{1}{2}\left(\frac{\zeta_{x'}^2}{\overline{\zeta_u^2}}+\frac{\zeta_{y'}^2}{\overline{\zeta_c^2}}\right)\right], \tag{11}$$

where $\overline{\zeta_u^2}$ and $\overline{\zeta_c^2}$ are the mean square slopes in the upwind and downwind directions, respectively, which can be determined by Eq. (8), and $|R_{\text{eff}}|^2$ are the effective reflection coefficients.

At a medium incidence angle, the breaking-wave scattering is also a significant non-Bragg scattering mechanism. Phillips ignored the specific mechanism of breaking-wave scattering and proposed a statistics model to describe non-Bragg scattering related to wave breaking (Phillips, 1988). It was considered that the overall contribution of wave breaking to backscattering cross-section depends on the scattering area of the breaking-wave

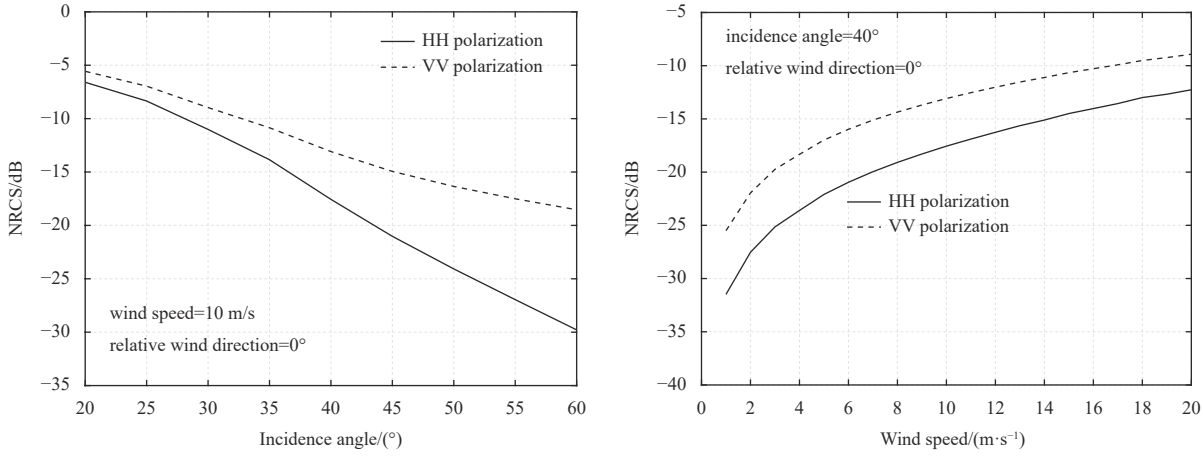

Fig. 2. Simulated normalized radar cross-section (NRCS) of composite Bragg scattering model versus radar incidence angle and wind speed. Solid line represents the NRCS of HH polarization, dashed line represents the NRCS of VV polarization.

front, and the relationship is as follows:

$$\sigma_{wb} = \int C(k/K, \theta, \varphi)\, k^{-1} \Lambda\left(\vec{k}\right) \mathrm{d}\vec{k}, \tag{12}$$

where $\Lambda\left(\vec{k}\right)\mathrm{d}\vec{k}$ is the length of the breaking-wave front per unit area to the wave number range $\vec{k}$ to $\vec{k}+\mathrm{d}\vec{k}$; The scattering area is proportional to $k^{-1}\Lambda\left(\vec{k}\right)\mathrm{d}\vec{k}$; and $C(k/K, \theta, \varphi)$ is an empirical function. Based on the proportional relationship between $\Lambda\left(\vec{k}\right)$ and $g^{-3/2}k^{1/2}u_*^3$, Eq. (11) can be simplified as follows:

$$\sigma_{wb}(\theta, \varphi) = C(\theta, \varphi)\left(\frac{u_*^2 K}{g}\right)^{3/2}. \tag{13}$$

However, it is difficult to determine the $C(\theta, \varphi)$ function by using meteorological observation. For actual sea surface, it is still impossible to determine and distinguish the occurrence conditions, specific contributions, and dominant mechanisms of each scattering mechanism under different sea conditions and radar parameters.

3 Results

3.1 *Scattering term of breaking waves*

A number of studies revealed that the composite scattering models, such as the CB model and TSM model, cannot fully describe and interpret the radar echo characteristics of the sea surface at a medium incidence angle. It is reported that there is a gross underestimate of predicted NRCS at large incident angles for HH polarization. It is generally believed that these anomalies are related to wave breaking. To further explore the wave-breaking scattering, a semi-empirical model (K19 model for short) is derived to quantitatively estimate the contributions of breaking waves to sea-surface total scattering (Kudryavtsev et al., 2005; Kudryavtsev et al., 2019).

For co-polarization:

$$\sigma_{wb}^{np}(\theta, U_{10}, \varphi) = f_{np}(\theta) U_{10}^{n_{np}} \exp(A_{0np} + A_{1np}\cos\varphi + A_{2np}\cos 2\varphi), \tag{14}$$

where

$$\begin{cases} n_{np}(\theta) = 1.3 + 4.7\times 10^{-2}(\theta - 30) \\ A_{0np} = 0.24 - 1.4\times 10^{-2}(\theta - 30) \\ A_{1np} = 0.33 + 1.3\times 10^{-2}(\theta - 30) \\ A_{2np} = 0.12 + 1.4\times 10^{-2}(\theta - 30) \\ f_{np}(\theta) = 1.9\times 10^{-3}\exp[-0.32(\theta - 30) + \\ \qquad 3.7\times 10^{-3}(\theta - 30)] \end{cases}. \tag{15}$$

For cross-polarization:

$$\sigma_{wb}^{cp}(\theta, U_{10}, \varphi) = f_{cp}(\theta) U_{10}^{n_{cp}} \exp(A_{0cp} + A_{1cp}\cos\varphi + A_{2cp}\cos 2\varphi), \tag{16}$$

where

$$\begin{cases} n_{cp}(\theta) = 2.4 + 1.5\times 10^{-2}(\theta - 30) \\ A_{0cp} = 0 \\ A_{1cp} = 10^{-2}(\theta - 30) \\ A_{2cp} = 0.12 \\ f_{cp}(\theta) = 2.5\times 10^{-6}\exp[-0.06(\theta - 30)] \end{cases}, \tag{17}$$

where σ_{wb}^{np} and σ_{wb}^{cp} are the NRCS induced by breaking waves for co-polarization and cross-polarization, respectively. Here, θ is the radar incidence angle; U_{10} is the wind speed at 10 m above the ocean surface; and φ is the relative wind direction.

To perform a quantitative evaluation to wave-breaking scattering, the NRCS of the wave-breaking term is compared with wind speed and relative wind direction, as shown in Fig. 3. It is clear that wave-breaking scattering can reach –20 dB with wind speeds above 10 m/s for co-polarization. Notice that the simulated NRCS induced by wave breaking achieved 72% of simulated NRCS using the CB model.

3.2 *A novel scattering model with breaking term*

To investigate a precise description of the sea-surface backscattering status, several numerical models were proposed in previous studies. In composite scattering theory, it has been found that any single scattering model cannot represent the scattering status of the sea surface, which results in a big bias when compared with satellite measurement results (Mouche et al., 2006; Voronovich and Zavorotny, 2011). Moreover, the "sea spike" feature in the high-resolution SAR image and a remarkable underes-

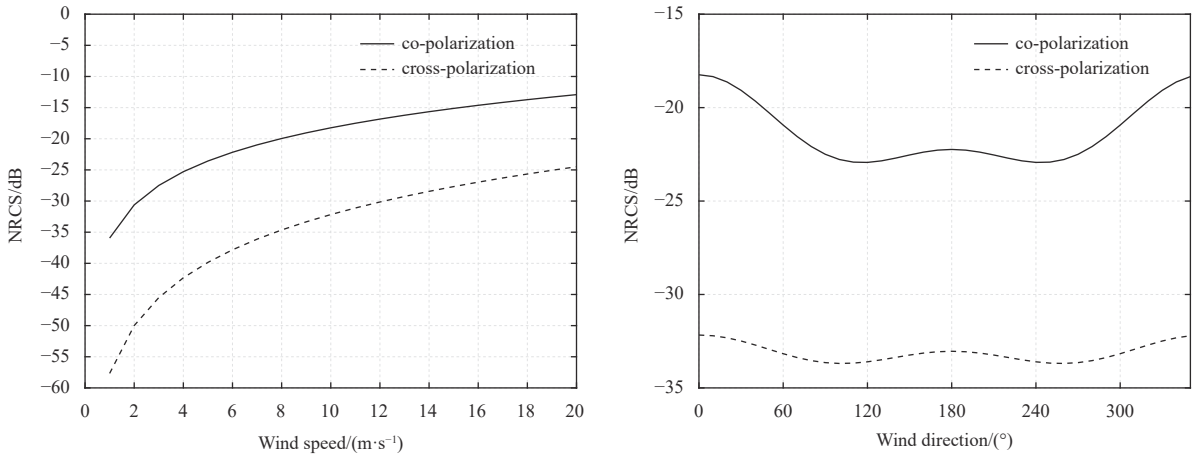

Fig. 3. Simulated normalized radar cross section (NRCS) induced by wave breaking versus wind speed and relative wind direction. The solid line represents the co-polarization and the dashed line represents the cross-polarization.

timation for HH polarization at intermediate and large incidence angles are not well explained (Voronovich and Zavorotny, 2001). To develop a novel scattering model for sea surface, the weight of the composite scattering terms is considered. In addition, a scattering term for wave breaking is proposed to explain the inaccurate expression of known scattering models, especially for HH polarization at intermediate and large incidence angles.

According to the composite scattering theory, a novel scattering model is proposed in this study, which is given as follows:

$$\sigma_0^p = \left(\sigma_{sp} + p\sigma_{br}^p\right)(1-q) + \sigma_{wb}q, \tag{18}$$

where σ_{sp} represents the quasi-specular scattering term; the σ_{br}^p represents the Bragg scattering term; and the σ_{wb} represents the wave-breaking scattering term. A factor p, related to the incidence angle and wind speed, is expressed as the contribution of Bragg scattering to total scattering of sea surface. The factor p can be attributed to the weight component of the Bragg scattering term on total sea-surface scattering. Parameter q represents the wave-breaking rate. Then, the statistical characteristics of sea-surface scattering can be presented as two parts: a weighted "ordinary" sea-surface scattering term and the weighted wave-breaking term.

It is noted that the wave-breaking rate q, can be determined with confirmation of the wave-breaking scattering term using Eqs (13) and (17). Then, the relationship between wave breaking rate and wind speed is shown in Fig. 4. The wave-breaking rate derived from the K19 model is compared with the K03 model. As shown in the figure, the wave breaking rate of the K19 model is slightly higher than the K03 model. The wave-breaking rate can achieve 35%–37% for wind speeds above 20 m/s.

With the second term of Eq. (17) confirmed, the weight factor of Bragg scattering can be acquired from the difference between $\sigma_0^{\mathrm{HH}}$and σ_0^{VV}. Using collected GF-3 SAR wave mode imagery, the relationship between weight factor p and radar parameters (incidence angle, polarization), wind vector (wind speed, relative wind direction) can be proposed by empirical fitting. Then the novel scattering model for sea surface with consideration of wave breaking can be derived from Eq. (17). It is found that the contribution of pure Bragg scattering drops to 45%–50% when the wind speed is above 10 m/s at a 40°–41° incidence angle. Obviously, the wave breaking plays a more important role in the novel model.

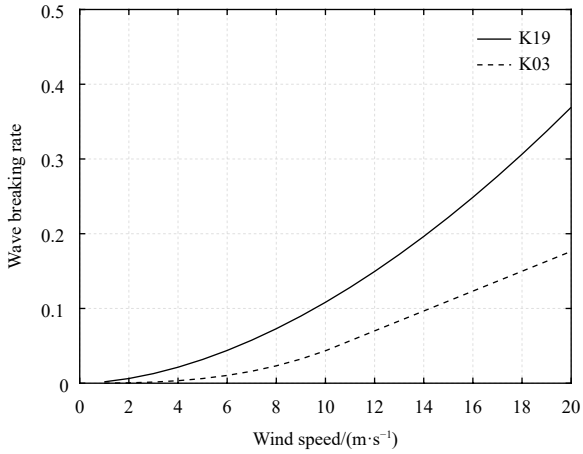

Fig. 4. Wave-breaking rate with increasement of wind speed. The solid line represents the K19 model; the dashed line represents the K03 model.

It is noticed that the wave-braking scattering component is approximately equal to the Bragg scattering component in conditions of wind speeds above 10 m/s. To reveal the scattering characteristics of our model, a comparison between the TSM model, CB model, and our model of incidence for HH and VV polarization at upwind and crosswind directions is shown in Fig. 5. Using the CB model, pure Bragg model, and our model, the simulated NRCSs of the HH and VV polarization are derived in conditions of upwind, crosswind, and downwind. The radar incidence angle was set to 40°.

3.3 *Validation*

To explore the modeling accuracy of sea-surface scattering, the simulated NRCS using our model and the measured NRCS using the matched GF-3 dataset were compared, as shown in Fig. 6. The comparison between the simulated NRCS from CMOD5.N and our model was given in Table 1. It is revealed that the performance of the VV polarization of our model is better than that of the HH polarization, with a correlation of 0.91, bias of –0.14 dB, root mean square error (RMSE) of 1.26 dB, and scattering index (SI) of –0.11.

Moreover, the geophysical models have demonstrated an accurate empirical relationship between the NRCS and wind speed, relative wind direction, and radar incidence angle, which are widely used for wind speed retrieval. For C-band, the corresponding geophysical model (GMF) models (e.g., CMOD4, CMOD5, CMOD5.N, CMOD7) were developed based on satellite-measured data. To validate our model precision, we compared the GMF of CMODs and our model with the NRCS of satellite-measured data from the GF-3 SAR wave mode imagery. For an incidence angle of 40°–41°, the relationship between the NRCS and wind speed, relative wind direction is shown in Fig. 7. It is easy to see that the proposed model performed much better than CMOD functions, especially for high wind speeds. In a previous study, it was shown that CMOD functions can show good performance for moderate wind speeds. However, a large bias is presented between different CMOD models in both low wind speed zones (less than 5 m/s) and high wind-speed zones (more than 20 m/s). Due to the saturation of SAR imagery, the satellite-measured NRCS will not raise with increasing wind speeds, especially in extreme sea states of typhoon conditions (Shao et al., 2019, 2017). Otherwise, in conditions of low wind speeds, the NRCS of satellites measured below the noise equivalent SIGMA0 (NE-SIGMA0), can be neglected as the noise in SAR echoes from the sea surface. Hence, the bias in conditions of low wind speeds can be well explained, as shown in Figs 7a and b. The comparison results are also listed in Table 2. As shown with Fig. 6, the performance of VV polarization is much better than HH polarization, with a correlation of 0.99, bias of –0.25 dB, RMSE of 0.64 dB, and SI of –0.04.

4 Discussion

Although the proposed model performed much better than the pure Bragg, CB, and CMOD models, the RMSE between our model and the measured NRCS could reach 2.53 dB and 1.26 dB, respectively. We attribute the inconsistency of the NRCS between the simulated and measured models to the sea states. In terms of wave-breaking scattering, effective observation is still lacking to confirm the scattering contribution of wave breaking to total scattering echo from sea surface. In addition to wave breaking, the sea states also significantly influence the NRCS from sea surface. Generally, the PO, GO, CB, TSM, MSM, SSA, and IEM take wind vector (wind speed, wind direction) as input, which ignores

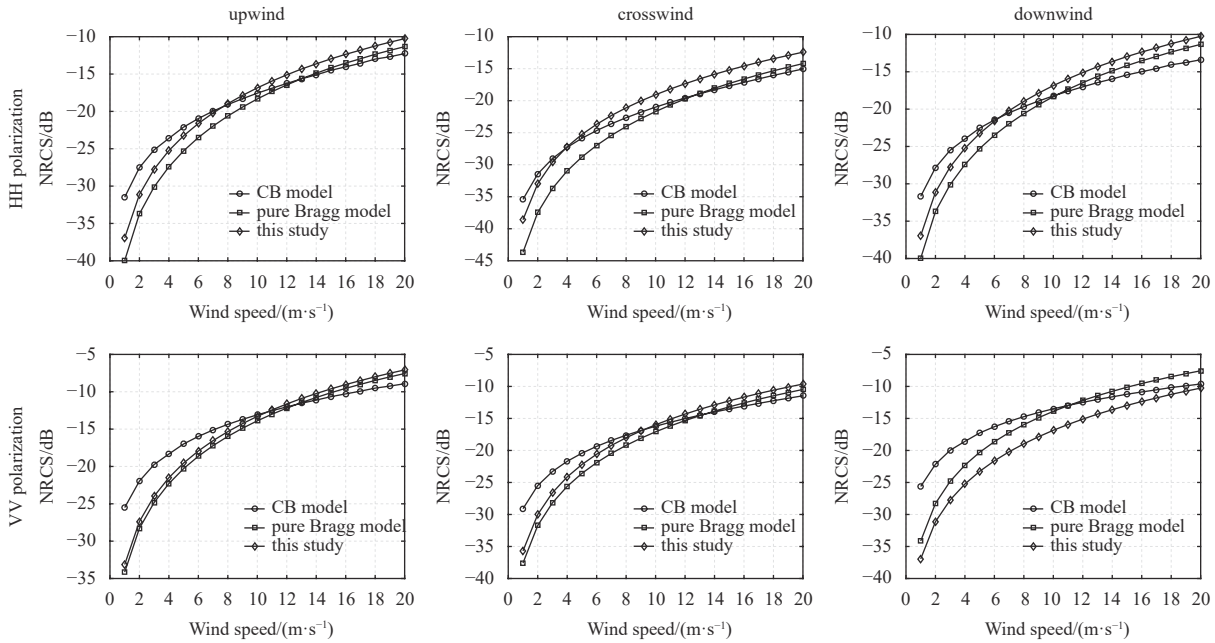

Fig. 5. Comparison of normalized radar cross section (NRCS) between different scattering models. The circle-marked solid line represents the composite Bragg (CB) model, the square-marked solid line represents the pure Bragg model, and the prism-marked solid line represents our proposed model.

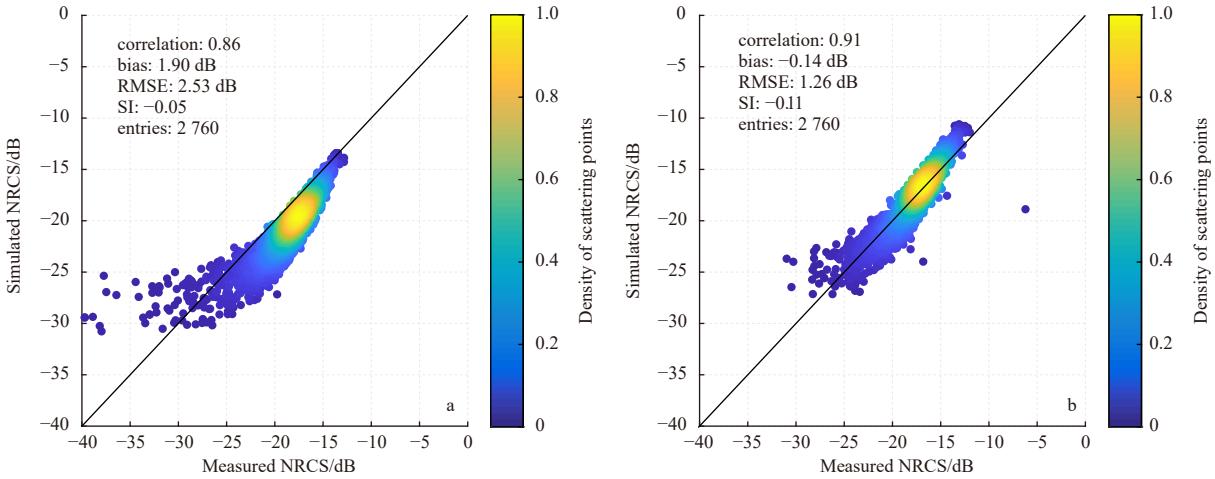

Fig. 6. Simulated normalized radar cross section (NRCS) using our proposed model compared with GF-3 observation. a. HH polarization; b. VV polarization. The solid line represents the one-to-one line.

Table 1. Comparison between the simulated normalized radar cross section from CMOD5.N and GF-3 measurement

Polarization	Correlation	Bias/dB	RMSE/dB	SI	Entries
HH	0.86	1.90	2.53	−0.05	2 760
VV	0.91	−0.14	1.26	−0.11	2 760

the effect of modulation of swell waves and current to wind-induced gravity-capillary waves (Kudryavtsev et al., 2014; Mouche et al., 2017). To explore the influence of swell waves and current on electromagnetic scattering from sea surface, the modulation relationship needs to be derived from the wave energy spectrum balance equation. The swell impact on SAR ocean wind retrievals and sea surface scattering were proposed in recent study. It is important to develop the wind and wave parameters retrieval precision with consideration of effect of modulation of swell waves (Wang et al., 2021; Li et al., 2019a; Stopa et al., 2017). In a future study, we will aim to compensate for the effect of swell wave and current to develop the empirical scattering model proposed in this work.

5 Conclusions

In this study, a novel SAR scattering model for a sea surface with breaking waves is proposed. Compared with existing models, the novel model considers an empirical relationship between wind speed and wave-breaking scattering to present the contribution of wave breaking. To explore the influence of different scattering mechanisms on SAR-measured NRCS, the scattering weight factor p and wave-breaking rate q, are performed to obtain the contribution of the quasi-specular scattering term, Bragg scattering term, and wave breaking scattering term to the total

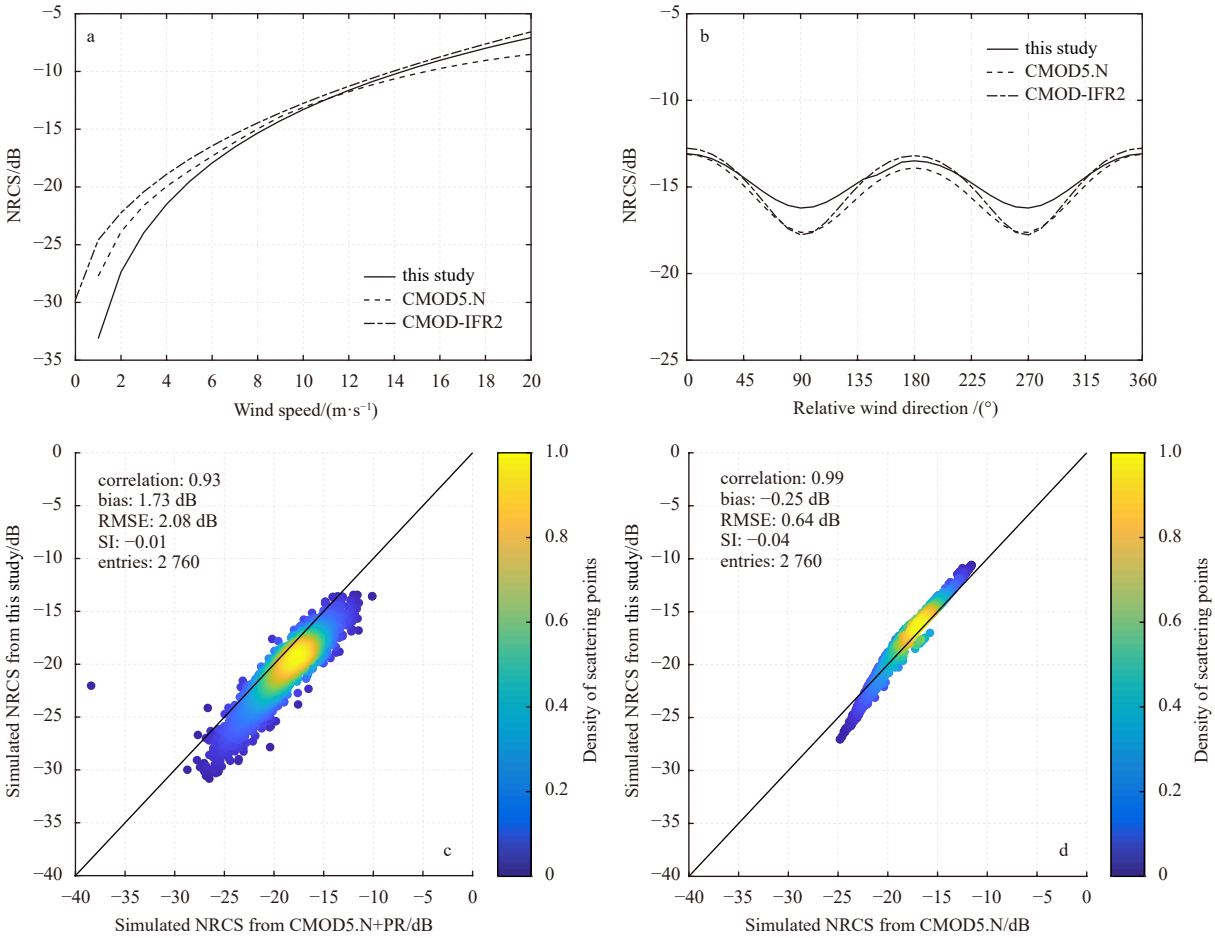

Fig. 7. Comparison between the proposed model and the CMOD model. a. Normalized radar cross section (NRCS) in VV polarization versus wind speed. b. NRCS in VV polarization versus wind direction. The solid line represents our proposed model; the dotted line represents the CMOD5.N model and CMOD-IFR2 model. c. Satellite-measured HH polarization NRCS with this study relative to CMOD5.N+PR. d. Satellite-measured VV polarization NRCS with this study relative to CMOD5.N.

Table 2. Comparison between the simulated normalized radar cross section from CMOD5.N and this study

Polarization	Correlation	Bias/dB	RMSE/dB	SI	Entries
HH	0.93	1.73	2.08	−0.01	2 760
VV	0.99	−0.25	0.64	−0.04	2 760

scattering from the sea surface.

To explore the modeling accuracy of sea-surface scattering, the simulated NRCS using the proposed model and measured NRCS (using the matched GF-3 dataset) were compared. It is revealed that the VV polarization of our model performs much better than does the HH polarization, with a correlation of 0.91, bias of –0.14 dB, RMSE of 1.26 dB, and SI of –0.11. Moreover, we compared the GMF of CMODs and our model, together with the satellite-measured NRCS from GF-3 SAR wave mode imagery. For an incidence angle 40°–41°, the relationship between the NRCS and wind speed, relative wind direction is proposed. Similar to the SAR-measured NRCS, the performance of VV polarization is much better than HH polarization, with a correlation of 0.99, bias of –0.25 dB, RMSE of 0.64 dB, and SI of –0.04. To develop the model precision, the wave-breaking scattering model should be quantitatively assessed in future studies. Moreover, other sea states (such as swell wave and current) should be considered in the scattering model for sea surface.

References

Apel J R. 1994. An improved model of the ocean surface wave vector spectrum and its effects on radar backscatter. Journal of Geophysical Research: Oceans, 99(C8): 16269–16291, doi: 10.1029/94JC00846

Barrick D E. 1965. A more exact theory of backscattering from statistically rough surfaces. Columbus, Ohio: The Ohio State University Research Foundation

Barrick D, Bahar E. 1981. Rough surface scattering using specular point theory. IEEE Transactions on Antennas & Propagation, 29(5): 798–800

Chubb S R, Cooper A L, Jansen R W, et al. 1999. Radar backscatter from breaking waves in Gulf Stream current convergence fronts. IEEE Transactions on Geoscience and Remote Sensing, 37(4): 1951–1966, doi: 10.1109/36.774707

Churyumov A N, Kravtsov Y A. 2000. Microwave backscatter from mesoscale breaking waves on the sea surface. Waves in Random Media, 10(1): 1–15, doi: 10.1088/0959-7174/10/1/301

Donelan M A, Pierson W J Jr. 1987. Radar scattering and equilibrium ranges in wind-generated waves with application to scatterometry. Journal of Geophysical Research: Oceans, 92(C5): 4971–5029, doi: 10.1029/JC092iC05p04971

Elfouhaily T, Chapron B, Katsaros K, et al. 1997. A unified directional spectrum for long and short wind-driven waves. Journal of Geophysical Research: Oceans, 102(C7): 15781–15796, doi: 10.1029/97JC00467

Gao Dong, Liu Yongxin, Meng Junmin, et al. 2018. Estimating significant wave height from SAR imagery based on an SVM regres-

sion model. Acta Oceanologica Sinica, 37(3): 103–110, doi: 10.1007/s13131-018-1203-7

Hauser D, Caudal G. 1995. Behavior of the ocean radar cross-section at low incidence, observed in the vicinity of the Gulf Stream. IEEE Transactions on Geoscience and Remote Sensing, 33(1): 162–171, doi: 10.1109/36.368212

Hauser D, Caudal G. 1996. Combined analysis of the radar cross-section modulation due to the long ocean waves around 14° and 34° incidence: Implication for the hydrodynamic modulation. Journal of Geophysical Research: Oceans, 101(C11): 25833–25846, doi: 10.1029/96JC02124

Hauser D, Caudal G, Guimbard S, et al. 2008. A study of the slope probability density function of the ocean waves from radar observations. Journal of Geophysical Research: Oceans, 113(C2): C02006

Helluy P, Golay F, Caltagirone J P, et al. 2005. Numerical simulations of wave breaking. ESAIM: Mathematical Modelling and Numerical Analysis, 39(3): 591–607, doi: 10.1051/m2an:2005024

Hwang P A, Plant W J. 2010. An analysis of the effects of swell and surface roughness spectra on microwave backscatter from the ocean. Journal of Geophysical Research: Oceans, 115(C4): C04014

Hwang P A, Zhang Biao, Toporkov J V, et al. 2010. Comparison of composite Bragg theory and quad-polarization radar backscatter from RADARSAT-2: With applications to wave breaking and high wind retrieval. Journal of Geophysical Research: Oceans, 115(C8): C08019

Kudryavtsev V, Akimov D, Johannessen J, et al. 2005. On radar imaging of current features: 1. Model and comparison with observations. Journal of Geophysical Research: Oceans, 110(C7): C07016

Kudryavtsev V N, Fan Shengren, Zhang Biao, et al. 2019. On quad-polarized SAR measurements of the ocean surface. IEEE Transactions on Geoscience and Remote Sensing, 57(11): 8362–8370, doi: 10.1109/TGRS.2019.2920750

Kudryavtsev V, Hauser D, Caudal G, et al. 2003. A semiempirical model of the normalized radar cross-section of the sea surface 1. Background model. Journal of Geophysical Research: Oceans, 108(C3): FET 2-1–FET 2-24

Kudryavtsev V, Kozlov I, Chapron B, et al. 2014. Quad-polarization SAR features of ocean currents. Journal of Geophysical Research: Oceans, 119(9): 6046–6065, doi: 10.1002/2014JC010173

Li Huimin, Mouche A, Stopa J E. 2019a. Impact of sea state on wind retrieval from Sentinel-1 wave mode data. IEEE Journal of Selected Topics in Applied Earth Observations and Remote Sensing, 12(2): 559–566, doi: 10.1109/JSTARS.2019.2893890

Li Huimin, Mouche A, Stopa J E, et al. 2019b. Calibration of the normalized radar cross section for Sentinel-1 wave mode. IEEE Transactions on Geoscience and Remote Sensing, 57(3): 1514–1522, doi: 10.1109/TGRS.2018.2867035

Mouche A A, Chapron B, Reul N, et al. 2007. Importance of the sea surface curvature to interpret the normalized radar cross section. Journal of Geophysical Research: Oceans, 112(C10): C10002, doi: 10.1029/2006JC004010

Mouche A A, Chapron B, Zhang Biao, et al. 2017. Combined co- and cross-polarized SAR measurements under extreme wind conditions. IEEE Transactions on Geoscience and Remote Sensing, 55(12): 6746–6755, doi: 10.1109/TGRS.2017.2732508

Mouche A A, Hauser D, Kudryavtsev V. 2006. Radar scattering of the ocean surface and sea-roughness properties: A combined analysis from dual-polarizations airborne radar observations and models in C band. Journal of Geophysical Research: Oceans, 111(C9): C09004

Phillips O M. 1988. Radar returns from the sea surface—Bragg scattering and breaking waves. Journal of Physical Oceanography, 18(8): 1065–1074, doi: 10.1175/1520-0485(1988)018<1065:RRFTSS>2.0.CO;2

Plant W J. 1986. A two-scale model of short wind-generated waves and scatterometry. Journal of Geophysical Research: Oceans, 91(C9): 10735–10749, doi: 10.1029/JC091iC09p10735

Plant W J. 2002. A stochastic, multiscale model of microwave backscatter from the ocean. Journal of Geophysical Research, 107(C9): 3120, doi: 10.1029/2001JC000909

Plant W J, Irisov V. 2017. A joint active/passive physical model of sea surface microwave signatures. Journal of Geophysical Research: Oceans, 122(4): 3219–3239, doi: 10.1002/2017JC012749

Romeiser R, Alpers W, Wismann V. 1997. An improved composite surface model for the radar backscattering cross section of the ocean surface: 1. Theory of the model and optimization/validation by scatterometer data. Journal of Geophysical Research: Oceans, 102(C11): 25237–25250, doi: 10.1029/97JC00190

Shao Weizeng, Ding Yingying, Li Jichao, et al. 2019. Wave retrieval under typhoon conditions using a machine learning method applied to Gaofen-3 SAR imagery. Canadian Journal of Remote Sensing, 45(6): 723–732, doi: 10.1080/07038992.2019.1683444

Shao Weizeng, Sheng Yexin, Sun Jian. 2017. Preliminary assessment of wind and wave retrieval from Chinese Gaofen-3 SAR imagery. Sensors, 17(8): 1705, doi: 10.3390/s17081705

Stopa J E, Mouche A A, Chapron B, et al. 2017. Sea state impacts on wind speed retrievals from C-Band radars. IEEE Journal of Selected Topics in Applied Earth Observations and Remote Sensing, 10(5): 2147–2155, doi: 10.1109/JSTARS.2016.2609101

Voronovich A. 1994. Small-slope approximation for electromagnetic wave scattering at a rough interface of two dielectric half-spaces. Waves in Random Media, 4(3): 337–367, doi: 10.1088/0959-7174/4/3/008

Voronovich A G, Zavorotny V U. 2001. Theoretical model for scattering of radar signals in Ku- and C-bands from a rough sea surface with breaking waves. Waves in Random Media, 11(3): 247–269

Voronovich A G, Zavorotny V U. 2011. Depolarization of microwave backscattering from a rough sea surface: Modeling with small-slope approximation. In: Proceedings of the 2011 IEEE International Geoscience and Remote Sensing Symposium. Vancouver, BC: IEEE, 2033–2036

Wang He, Li Huimin, Lin Mingsen, et al. 2019. Calibration of the co-polarized backscattering measurements from Gaofen-3 synthetic aperture radar wave mode imagery. IEEE Journal of Selected Topics in Applied Earth Observations and Remote Sensing, 12(6): 1748–1762, doi: 10.1109/JSTARS.2019.2911922

Wang He, Yang Jingsong, Zhu Jianhua, et al. 2021. Estimation of significant wave heights from ASCAT scatterometer data via deep learning network. Remote Sensing, 13(2): 195, doi: 10.3390/rs13020195

Wu S T, Fung A K. 1972. A noncoherent model for microwave emissions and backscattering from the sea surface. Journal of Geophysical Research, 77(30): 5917–5929, doi: 10.1029/JC077i030p05917

Yan Qiushuang, Zhang Jie, Fan Chenqing, et al. 2018. Study of sea-surface slope distribution and its effect on radar backscatter based on Global Precipitation Measurement Ku-band precipitation radar measurements. Journal of Applied Remote Sensing, 12(1): 016006

Zhang Tianyu, Li Xiaoming, Feng Qian, et al. 2019. Retrieval of sea surface wind speeds from Gaofen-3 full polarimetric data. Remote Sensing, 11(7): 813, doi: 10.3390/rs11070813

Zhang Biao, Zhao Xiaolu, Perrie W, et al. 2020. On modeling of quad-polarization radar scattering from the ocean surface with breaking waves. Journal of Geophysical Research: Oceans, 125(8): e2020JC016319

Zhong Lihua, Qiu Xiaolan, Han Bing, et al. 2020. An improved descalloping method combined with imaging parameters for GaoFen-3 ScanSAR. Remote Sensing, 12(5): 822, doi: 10.3390/rs12050822